

# Forcing-dependent stability of steady turbulent states

B. Saint-Michel,<sup>1,\*</sup> B. Dubrulle,<sup>1</sup> F. Ravelet,<sup>2</sup> and F. Daviaud<sup>1</sup>

<sup>1</sup>*Laboratoire SPHYNX, Service de Physique de l'État Condensé,  
DSM, CEA Saclay, CNRS URA 2464, 91191 Gif-sur-Yvette, France*

<sup>2</sup>*Laboratoire Dynfluid, ENSAM ParisTech, CNRS EA92, 151, boulevard de l'Hôpital 75013 Paris, France*  
(Writing in progress: January 10, 2013)

We study the influence of the forcing on the steady turbulent states of a von Kármán swirling flow, at constant impeller speed, or at constant torque. We find that the different forcing conditions change the nature of the stability of the steady states and reveal dynamical regimes that bear similarities with low-dimensional systems. We suggest that this forcing dependence may be an out-of-equilibrium analogue of the *ensemble inequivalence*, valid for long-range interacting statistical systems, and that it may be applicable to other turbulent systems.

PACS numbers: 47.20.Ky, 05.45.-a, 47.27.Sd

**Introduction** An intriguing property of statistical systems with long range interactions is the *ensemble inequivalence*: a solution in the microcanonical (constrained) ensemble is not necessarily a solution in the canonical (unconstrained) ensemble [1, 2]. This property traces back to the non-additivity of energy, and is reflected by pathological behaviours of the entropy (that can be non-concave) or the heat capacity (that can become negative). Ensemble inequivalence has been observed and studied in a variety of systems such as for example 2D Euler equations [3, 4], Blume-Emery-Griffiths model [5], random graphs [6]. More recently, it has also been studied in a model describing the one-dimensional motion of  $N$  rotators coupled through a mean-field interaction, and subjected to the perturbation of an external magnetic field [7]; it shows that this concept may also hold out of equilibrium, broadening its range of applicability. Nevertheless, a generalisation of such concepts to all out-of-equilibrium systems remains — at present time — an open question. We propose an extension of such tools to turbulent systems. They naturally display long-range interactions and are, by definition, far from equilibrium. Our experimental system is a “von Kármán” experiment, in which a cylinder of fluid is stirred by two impellers with blades, producing fully-developed turbulence in a relatively small experimental device. Several features of equilibrium systems have already been described in this model experiment, such as steady states, predicted by the resolution of the axisymmetric Euler equations [8], hysteresis [9], and spontaneous symmetry-breaking with diverging susceptibility [10].

In this letter, we will examine the stability of such steady states under two different forcing conditions, either imposing the *speed* or the *torque* to our impellers. The subject has attracted little attention, only focusing on the difference of power fluctuations [11, 12] under both conditions. However, we can consider our forcings to be conjugate, as the product torque  $\times$  speed controls the energy injection rate in our experiment. Switching from speed to torque control might then be seen as an analogue

of switching from *canonical* to *microcanonical* ensemble; it is shown to alter the stability of the steady states previously observed in [9] and to reveal interesting dynamical regimes.

**Experimental setup** The von Kármán flow is created in a Polycarbonate cylinder of radius  $R = 100$  mm filled with water. The fluid is stirred by two 8-bladed impellers of radius  $0.925R$  separated from each other by a distance (blade-tip to blade-tip)  $2h = 1.4R$  (see fig. 1). Two independent 1.8 kW brush-less motors can rotate the impellers by imposing torque – or speed – to the system. The fluid is confined in the cylinder by two balanced mechanical seals under a  $P = 2.8$  bar pressure to ensure minimum friction. Two torque sensors measure the rotation angle – and therefore the speed – and the torque applied on the two impellers, respectively  $(f_1, C_1)$  and  $(f_2, C_2)$ . Temperature control is enforced by an external water flow in two refrigeration coils installed behind each impeller. We define the Reynolds number of our experiment as  $Re = \frac{\pi(f_1+f_2)R^2}{\nu}$ , varying from  $2 \cdot 10^5$  to  $5 \cdot 10^5$  depending on the speed of the impellers. Furthermore, we define two main parameters, each corresponding to the control parameter of one type of experiment:

- $\theta = \frac{f_1-f_2}{f_1+f_2}$ , the reduced impeller *speed* difference for the experiments where  $2f_0 = f_1 + f_2 = 8$  Hz is imposed;
- $\gamma = \frac{C_1-C_2}{C_1+C_2}$ , the reduced shaft *torque* difference for the experiments where  $2C_0 = C_1 + C_2 = 3.45$  Nm is imposed.

$f$  and  $C$  are conjugate quantities: for a given experiment, we either impose a torque  $C$  – respectively an impeller speed  $f$  – to measure the impeller frequency  $f$  – respectively the torque  $C$ . The product of these two quantities also defines the amount of power injected in the experiment,  $\mathcal{P} = 2\pi fC$ .

**Speed imposed** For speed-imposed experiments, a hysteresis cycle which opens for  $Re \geq 4000$  has been observed [9]. Fig. 2 depicts the torque-speed asymmetry

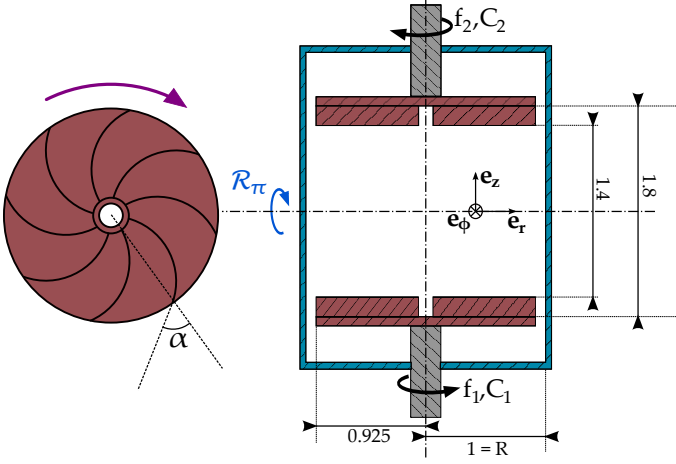


FIG. 1: Sketch of the ‘VK2’ experiment. *Left*: Impeller used for the experiment and blade profile: curvature  $\alpha = 72^\circ$ , blade height  $0.2R$ . *Right*: section of the experiment with the  $\mathcal{R}_\pi$  and  $(Oz)$  symmetries. The refrigeration coils are not shown.

relation  $\gamma(\theta)$ : starting both impellers at the same time for  $\theta$  very close to 0, the system remains steady in a ‘symmetric’ branch called  $(s)$ . A slight variation of  $\theta$  on this branch triggers a global bifurcation with a dramatic increase of the mean torque  $\frac{1}{2}(C_1 + C_2)$ . Two new, ‘bifurcated’ branches of the  $(\gamma, \theta)$  plane are created;  $(b_1)$  (mainly for  $\theta \geq 0$  and  $\gamma > 0$ ) and  $(b_2)$  (mainly for  $\theta \leq 0$  and  $\gamma < 0$ ) are exchanged by  $\mathcal{R}_\pi$  rotation.

These states have been characterized both by stereoscopic Particle Image Velocimetry (sPIV) and Laser Doppler Velocimetry (LDV): in  $(s)$ , each impeller generates one flow cell by Ekman recirculation. The two cells are separated by a shear layer, similarly as in [9, 10] for  $\theta = 0$ . In contrast, both bifurcated branches display only one circulation cell covering the entire system. PIV measurements have confirmed that  $(b_1)$  and  $(b_2)$  mean velocity fields are effectively images of each other by the  $\mathcal{R}_\pi$  rotation.

Once on  $(b_1)$  and  $(b_2)$  branches, it is never possible to reach again the  $(s)$  state, which is thus only observed while starting the impellers at the exact same time. In addition, the  $(b_1)$  and  $(b_2)$  branches are hysteretic,  $(b_1)$  being for example stable for  $\theta$  down to  $-0.15$ . Furthermore, a notable  $\gamma$  range  $[-0.089; -0.018] \cup [0.00; 0.055]$  is not accessible due to the separation of our three branches [13].

*Torque imposed* In contrast, imposing *torque* allows us to choose  $\gamma$ , assuming friction is negligible. For the values of  $\gamma$  accessible by imposing speed, the states reached are steady and we clearly see that the mean observed  $\theta$  is consistent with speed-imposed experiments.

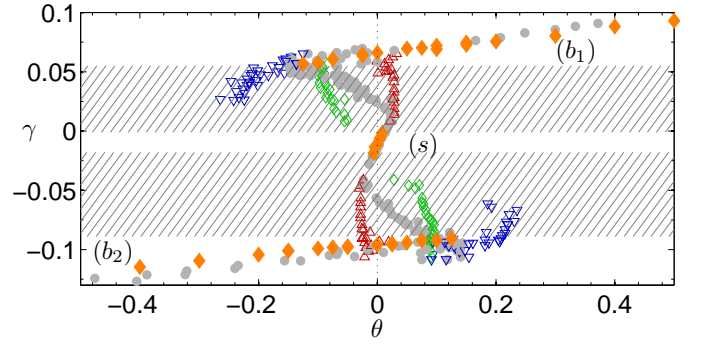


FIG. 2: Torque asymmetry parameter  $\gamma = \frac{C_1 - C_2}{C_1 + C_2}$  as a function of the speed asymmetry parameter  $\theta = \frac{f_1 - f_2}{f_1 + f_2}$ . Speed experiments ( $\diamond$ ) impose  $\theta$  to determine  $\gamma$ , whereas torque experiments ( $\bullet$ ) do the opposite. While a hysteresis cycle is observed in speed experiments, new ‘forbidden’ branches are observed. These branches are multistable, mixing slow bifurcated —  $(\tilde{b}_{1,2})$  — states ( $\nabla$ ), intermediate —  $(\tilde{i}_{1,2})$  — ( $\diamond$ ), and fast symmetrical state ( $\tilde{s}$ ) ( $\triangle$ ). The hatched region represents the inaccessible  $\gamma$  values imposing speed.

We will then assume that they are identical. This result has also been confirmed by PIV measures, with torque-driven and speed-driven velocity fields almost identical when properly normalised in both  $(s)$  and  $(b)$  branches. However,  $\gamma$  values from the forbidden region are now accessible. In such regions, the system loses its steadiness and transits between multiple turbulent states. The multi stability is characterized by the emergence of multiple peaks in the P.D.F. (probability density function) of  $\theta_f(t)$ , the 1.5 Hz low-pass filtered signal of  $\theta(t)$ . This filtering is required considering our speed measurements generate discrete values of the impeller speed  $f$ , and yield a robust density function when the filter cut-off frequency is changed. Therefore, three types of ‘attractor’ states have been defined:  $(\tilde{s})$ , the high-speed state, with characteristics similar to  $(s)$ ,  $(\tilde{b}_1)$  and  $(\tilde{b}_2)$  which are low-speed states similar to  $(b_1)$  and  $(b_2)$ , and two new  $(\tilde{i}_1)$  and  $(\tilde{i}_2)$  *intermediate* states. All of these states may hold longer ( $> 10$  sec.) than any characteristic time of our experiment for specific  $\gamma$  values inside the formerly forbidden zone. These new states can be seen in fig. 2; while  $(\tilde{s})$ ,  $(\tilde{b}_1)$   $(\tilde{b}_2)$  states extend well beyond their speed-imposed counterparts, the  $(\tilde{i}_1)$  and  $(\tilde{i}_2)$  branches are new and cannot be observed otherwise.

Decreasing  $\gamma$  from a perfectly symmetric  $(\tilde{s})$  ( $\theta = 0$ ) state, we can observe its influence on the temporal signals, (cf. fig. 3). First, the speed of the impellers remains steady. Then (fig. 3(b)), when  $\gamma \leq \gamma_{c1} \approx -0.049$  — corresponding to the extremum of  $\theta_-$ , small excursions towards  $(\tilde{i}_2)$  occur. For larger  $\gamma$ , the oscillations become larger and allow sometimes short jumps towards the  $(\tilde{b}_2)$  state (fig. 3(c)). In the region where all  $(\tilde{s})$ ,  $(\tilde{i}_2)$ ,  $(\tilde{b}_2)$  states are observed (fig. 3(d)), some ‘steady’

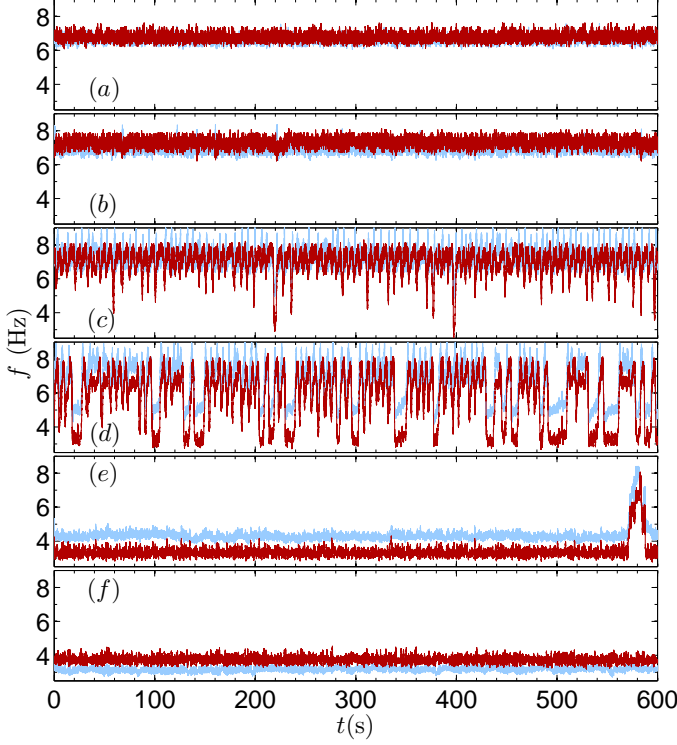


FIG. 3: Temporal series of the impeller speeds  $f_1$  (blue) and  $f_2$  (red) for various  $\gamma$ . (a), symmetric high-speed state ( $\tilde{s}$ ) observed at  $\gamma = -0.0164$ ; (b), threshold of the irregular oscillations ( $\tilde{i}_2$ ) with very small events for  $\gamma = -0.0460$ ; (c), ( $\tilde{i}_2$ ) irregular oscillations for  $\gamma = -0.0668$ ; (d), multi stable regime showing ( $\tilde{s}$ ), ( $\tilde{i}_2$ ) and ( $\tilde{b}_2$ ) events at  $\gamma = -0.0891$ ; (e), a single fast rare event in a quasi-steady slow ( $\tilde{b}_2$ ) regime at  $\gamma = -0.0912$ ; (f), slow ( $\tilde{b}_2$ ) regime for  $\gamma = -0.1049$ .

( $\tilde{i}_2$ ) events, exceeding 10 sec (70 impeller cycles), have been observed. Decreasing  $\gamma$  further affects this region by favouring ( $\tilde{b}$ ) at the expense of ( $\tilde{i}$ ) and ( $\tilde{s}$ ). Therefore, for low  $\gamma \geq \gamma_{c2} \approx -0.0920$  (fig. 3(e)), only rare events can drive the system to the ( $\tilde{i}_2$ ) state, and nearly no time is spent in the ( $\tilde{s}$ ) state. Eventually, the system joins the ( $\tilde{b}_2$ ) steady branch (fig. 3(f)) for  $\gamma \leq -0.099$ .

Valuable information on our system dynamics can be found studying the temporal signals of the global quantities near the transitions [14]. We have therefore superposed in fig. 4 the speed signals close to the transitions observed in fig. 3(c): ( $\tilde{s}$ )  $\rightarrow$  ( $\tilde{b}_{1,2}$ ) is called down, and ( $\tilde{b}_{1,2}$ )  $\rightarrow$  ( $\tilde{s}$ ) up. Once the transition times  $\tau_i$  accurately determined, a fair collapse of  $f_{1,2}([\tau_i - 5 \text{ sec.}; \tau_i + 3 \text{ sec.}])$  has been observed. It is therefore possible to deduce a general transition scenario for up and down transitions. The up transition seems to result from a correlated positive fluctuation of the two impellers, whereas the down one suggests a degenerate ( $\tilde{i}_2$ ) oscillation in which a sudden impeller correlation is triggered very close to  $\tau_i$ .

Eventually, the distribution of ( $f_1, f_2$ ) are studied to

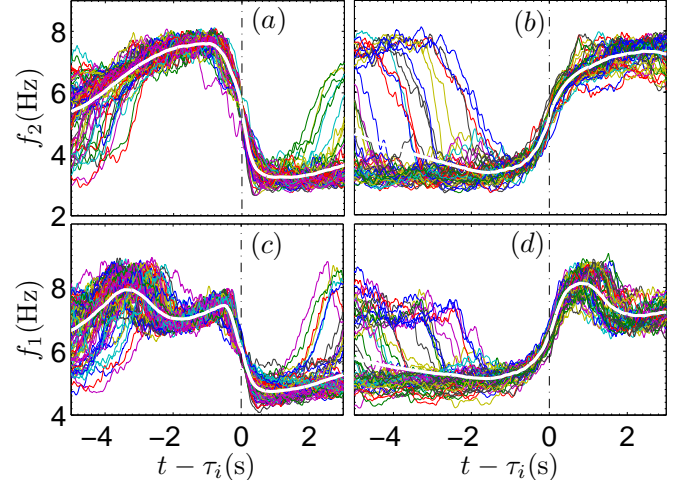


FIG. 4: Shifted temporal signals of 60 randomly-chosen transitions of a 2-hour experiment with  $\gamma = -0.0891$ . We compute  $\tau_i$  by finding the minimum of  $|\partial_t \tilde{f}_2|$  where  $\tilde{\cdot}$  means the  $\cdot$  signal has been numerically filtered at 1 Hz. (a), (c), respectively  $f_2$  and  $f_1$  profiles for down transitions. (b), (d), respectively  $f_2$  and  $f_1$  for  $\uparrow$  transitions. The thick white line represents in each sub-plot the rotation frequency averaged on all 195 events of the experiment,  $f^m$ .

characterise the attractor states that emerge from figs. 2 and 3. In fig. 5(a), for  $\gamma$  too small, only one peak appears, which confirms the steady nature of the system in ( $\tilde{s}$ ). For small asymmetries, small excursions that escape the attractor, corresponding to the previously described small ( $\tilde{i}_2$ ) oscillations can be found, exhibiting a new peak strongly deviating from the diagonal  $f_1 = f_2$ . For higher asymmetries, the system fills a large part of the ( $f_1, f_2$ ) plane, with three main maxima: ( $\tilde{s}$ ) close to the diagonal at higher ( $f_1, f_2$ ), ( $\tilde{b}_2$ ) for the off-diagonal low ( $f_1, f_2$ ) regime. The third — ( $\tilde{i}_2$ ) — attractor is harder to see because it is partially hidden by neighbouring zones repeatedly crossed by unsteady events. It is located roughly between the right tip of the joint histogram and the ( $\tilde{s}$ ) maximum. With this representation, one clearly observes that the mean system path is different for the down and up transitions: while the down transition seems to start “looping” in the vicinity of ( $\tilde{s}$ ) before abruptly transitioning to ( $\tilde{b}_2$ ), the up transition reaches the right edge of the joint-PDF ( $f_1 > f_2$ ), near ( $\tilde{i}_2$ ) before joining the ( $\tilde{s}$ ) state.

The repartition of the height of the maxima in fig. 5(c), (d), (e) is obviously driven by  $\gamma$ , from almost-fully ( $\tilde{s}$ ), ( $\tilde{i}_2$ ) to nearly-pure ( $\tilde{b}_2$ ) with rare large transitions to the faster states. For nearly-pure ( $\tilde{s}$ ), we clearly see (fig. 5(c)) that a large amount of excursions occur, contrasting with the nearly-pure ( $\tilde{b}_2$ ) state (fig. 5(e)), for which no excursion is observed (though a few transitions are). In addition, the position of these maxima is *not* fixed when  $\gamma$  is changed: indeed, we recall for example that fig. 2 shows a

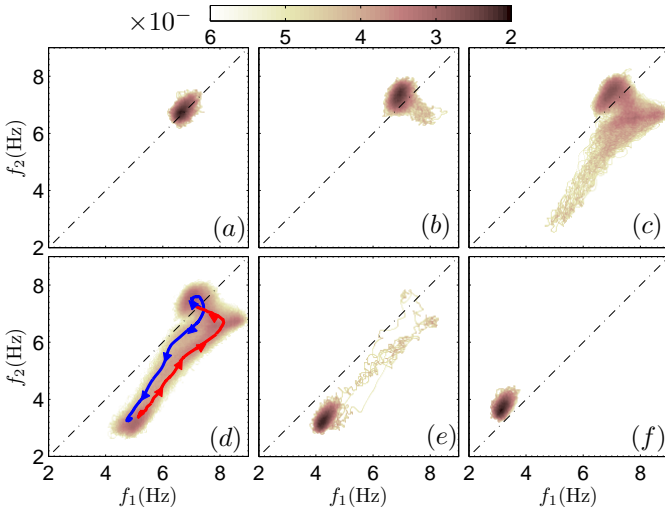


FIG. 5: Joint-probability density maps of the  $(f_1, f_2)$  values (log-scale), based on the temporal signals of fig. 3: (a), steady symmetric high-speed state:  $\gamma = -0.0164$ ; (b), beginning of irregularly oscillating states towards an intermediate state,  $\gamma = -0.0460$ ; (c), typical irregular oscillations with large slowdowns:  $\gamma = -0.0668$ ; (d), multistability with three ‘most visited’ states:  $\gamma = -0.0891$ , (—) and (—) represent respectively the fig. 4 mean profile for down and up transitions; (e), rare events for  $\gamma = -0.0912$ ; (f), steady slow state:  $\gamma = -0.1042$ . The black dashed-dotted line represents the  $\theta = 0$  condition. Both fast and slow states can be observed at  $\theta = 0$  considering the shape of the fig. 2 curve.

clear  $\theta$  variation of the steady  $(s)$ ,  $(b_{1,2})$  maxima when  $\gamma$  is increased. Interestingly, while the  $(\tilde{b})$  and  $(\tilde{s})$   $\theta$  values increase with  $\gamma$ , the  $(\tilde{i})$   $\theta$  position *decreases* with  $\gamma$ .

**Discussion** Using global torque and speed measurements, we have characterised the response of the von Kármán experiment to different energy injection mechanisms. The two responses coincide in the range of parameters accessible to the constant velocity forcing mode, corresponding to the hysteresis cycle previously reported by [9]. However, imposing the torque  $\gamma$  in the zone which could not be reached in speed experiments generate new continuous “mean” branches connecting symmetric  $(s)$  and bifurcated  $(b)$  branches. However, these “mean states” are not representative of the dynamics observed: the P.D.F of  $\bar{\theta}$  may exhibit up to three peaks, corresponding to “intermittent” states. Two of them can be defined by continuity with the speed-imposed states:  $(\tilde{s})$  and  $(\tilde{b})$ . The third state,  $(\tilde{i})$ , is never observed in any speed-imposed experiment. The study of the impellers velocity  $V_1(t), V_2(t)$  signals show typical excursions and transitions between our three states, similarly to [16, 17], while preliminary results on the distribution of  $(\tilde{b})$  residence time favour exponential Kramers-like escape times. It might then be possible to describe the evolution of our global quantities with a very simple model of ground states with noise, as performed by [18]. Work is also in

progress to characterize the geometry of the corresponding steady states through PIV measurements.

Our results address two questions. First, from the point of view of statistical physics, the von Kármán experiment allows a quantitative analysis of the influence of the energy injection on the response of an out-of-equilibrium system. Our forcings are conjugated with respect to the energy injection rate, equivalent in a steady case to an energy dissipation rate, or entropy production rate, and do not provide the same results: more “working states” are found when imposing torque. This is reminiscent of what happens in systems with long-range interactions, between the microcanonical (constant energy) case and the canonical (constant temperature) case. For a particular set of parameters, the microcanonical ensemble exhibits a negative specific heat region  $c_v = \frac{\partial E}{\partial T} < 0$ , despite continuous variation of  $T$ . Canonical ensemble cannot sustain such  $c_v < 0$  otherwise energy fluctuations in the system generate destabilizing heat transfer from the thermal reservoir. Therefore, a brutal first-order transition is observed, similar to our bifurcations in speed control, whereas torque control allows a continuous transition. More specific features point towards ensemble inequivalence in our system: a new quasi-steady solution,  $(\tilde{i})$ , arises only in torque control. In addition, positive  $\chi$  regions are found to be identical, “ensemble equivalent”, in both controls, whereas only torque control allows multiple portions of negative, “ensemble inequivalent”,  $\chi^{-1}(\gamma) = \frac{\partial \theta}{\partial \gamma}$ , which cannot be found in speed control. These results strongly recall those obtained with out-of-equilibrium rotators [7].

Second, from the point of view of turbulence, it sets the problem of *universality* of the steady states, that appears to be rather sensitive to the energy injection mechanisms, at variance with traditional view of turbulence. The phenomenon we explore in the present letter could actually be present in other turbulent experimental systems: for example, turbulent Plane-Couette flows could be forced either with constant global stress (motor torque  $C$ ) or global strain (speed  $f$ ), Poiseuille flows have been studied either imposing a pressure difference  $\Delta P$  or a mass flow-rate  $q_m$  [20], and even Rayleigh-Bénard experiments have been conducted under temperature-imposed ( $T$ ) and the heat-flux imposed ( $\partial_t Q$ ) conditions [21]. While the two first examples also exhibit a “duality” of the forcing types ( $\mathcal{P} = q_m \Delta P = Cf$ ), Rayleigh-Bénard experiments do not respect this condition ( $\mathcal{P} = \partial_t Q$ ). It is difficult to understand what would be the equivalents of  $\theta \neq 0$  and  $\gamma \neq 0$  in Poiseuille flows, but previous work on rotating Rayleigh-Bénard convection, which can be viewed as analogous to our  $\theta \neq 0$  experiments, has also shown interesting “chaotic” dynamics [22]. Last, we may wonder whether the forcing dependence is present in natural systems where such reversals are observed: northern hemisphere winds zonal and blocked [23] patterns, whereas Kuroshio currents [24] might deviate abruptly from their



initial course: both systems exhibit complex dynamics with jumps between quasi-steady states.

*Acknowledgements* We thank the CNRS and CEA for support, Vincent Padilla for building the experimental device and for mechanical advising, Guillaume Mancel for sharing most of the experimental data, and Cecile Wiertel-Gasquet for writing the programs and helping with the acquisition devices.

---

\* Electronic address: brice.saint-michel@cea.fr

- [1] W. Thirring, Z. Phys. A, **235**, 339-352 (1970)
- [2] R.S. Ellis, K. Haven and B. Turkington: Large Deviation Principles and Complete Equivalence and Nonequivalence Results for Pure and Mixed Ensembles. J. Stat. Phys. **101**, 999 (2000)
- [3] C. Herbert, B. Dubrulle, P.-H. Chavanis and D. Paillard, Phys. Rev. E, **85**, 5, 056304 (2012)
- [4] A. Venaille and F. Bouchet, Phys. Rev. Lett., **102**, 10, 104501 (2009)
- [5] J. Barré, D. Mukamel, S. Ruffo, Phys. Rev. Lett., **87**, 3, 030601 (2001); M.J. Blume, V.J. Emery, R.B. Griffiths, Phys. Rev. A, **4**, 1071-1077 (1971)
- [6] J. Barré and B. Goncalves, Physica A 386, 212-218 (2007).
- [7] G. De Ninno and D. Fanelli, Europhys. Lett., 97 20002 (2012).
- [8] R. Monchaux, F. Ravelet, B. Dubrulle, A. Chiffaudel and F. Daviaud, Phys. Rev. Lett., **96**, 12, 124502 (2006)
- [9] F. Ravelet, L. Marié, A. Chiffaudel and F. Daviaud, Phys. Rev. Lett., **93**, 16, 164501 (2004)
- [10] P.-P. Cortet, E. Herbert, A. Chiffaudel, F. Daviaud, B. Dubrulle and V. Padilla, J. Stat. Mech. Theor. Exp., **2011**, 07, P07012 (2011); P.-P. Cortet, A. Chiffaudel, F. Daviaud and B. Dubrulle, Phys. Rev. Lett., **105**, 214501 (2010)
- [11] J.H. Titon and O. Cadot, Phys. Fluids, **15**, 625 (2003)
- [12] N. Leprovost, L. Marié and B. Dubrulle, European Physical Journal B 39 (2004) 121-129
- [13] This range, as well as fig. 2 do not exactly respect  $\mathcal{R}_\pi$  symmetry. It is actually very difficult to obtain accurate symmetric calibrations because such experiments require small and accurate torques.
- [14] M. Berhanu, R. Monchaux, S. Fauve, N. Mordant, F. Pétrélis, A. Chiffaudel, F. Daviaud, B. Dubrulle, L. Marié, F. Ravelet, M. Bourgoin, Ph. Odier, J.-F. Pinton and R. Volk, Europhys. Lett., **77**, 5 (2007)
- [15] S. T. Bramwell, P. C. W. Holdsworth and J.-F. Pinton, Nature, **396**, 552-554 (1998)
- [16] F. Pétrélis and S. Fauve, J. Phys.: Condens. Matter, **20**, 494203 (2008)
- [17] F. Pétrélis, S. Fauve, E. Dormy and J.-P. Valet, Phys. Rev. Lett., **102**, 144503 (2009)
- [18] A. de la Torre and J. Burguete, Phys. Rev. Lett., **99**, 054101 (2007)
- [19] F. Ravelet, Ph.D. thesis, Ecole Polytechnique, 2005 (<http://www.imprimerie.polytechnique.fr/-Theses/Files/Ravelet.pdf>)
- [20] A. G. Darbyshire and T. Mullin, J. Fluid Mech, **289**, 3, 83-114 (1995)
- [21] H. Johnston and C. R. Doering, Phys. Rev. Lett., **102**, 6, 064501 (2009)
- [22] F. H. Busse and K. E. Heikes, Science, **208**, 4440, 173-175 (1980); Y. Tu and M. C. Cross, Phys. Rev. Lett., **69**, 17, 2515-2518 (1992)
- [23] R. Berggren, B. Bolin and C.-G. Rossby, Tellus, **1**, 2, 14-37 (1949); E. Weeks, Y. Tian, J. S. Urbach, K. Ide, H. L. Swinney and M. Ghil, Science, **278**, 5343, 1598-1601 (1997)
- [24] Kawabe, M., J. Phys. Oceanogr., **25**, 12, 3103-3117 (1995)